# Time–Temperature Indicator for Perishable Products Based on Kinetically Programmable Ag Overgrowth on Au Nanorods

**Chao Zhang,[†,‡] An-Xiang Yin,[†] Ruibin Jiang,[‡] Jie Rong,[§] Lu Dong,[§] Tian Zhao,[†] Ling-Dong Sun,[†,*] Jianfang Wang,[‡,*] Xing Chen,[§,*] and Chun-Hua Yan[†,*]**

[†]State Key Lab of Rare Earth Materials Chemistry and Applications, Peking University, Beijing 100871, China, [‡]Department of Physics, The Chinese University of Hong Kong, Shatin, Hong Kong SAR, China, and [§]College of Chemistry and Molecular Engineering, Peking University, Beijing 100871, China

**ABSTRACT** Food safety is a constant concern for humans. Besides adulteration and contamination, another major threat comes from the spontaneous spoilage of perishable products, which is basically inevitable and highly dependent on the temperature history during the custody chain. For advanced quality control and assessment, time–temperature indicators (TTIs) can be deployed to document the temperature history. However, the use of TTIs is currently limited by either relatively high cost or poor programmability. Here we describe a general, kinetically programmable, and cost-efficient TTI protocol constructed from plasmonic nanocrystals. We present proof-of-principle demonstrations that our TTI can be specifically tailored and thus used to track perishables, dynamically mimic the deteriorative processes therein, and indicate product quality through sharp-contrast multicolor changes. The flexible programmability of our TTI, combined with its substantially low cost and low toxicity, promises a general applicability to each single packaged item of a plethora of perishable products.

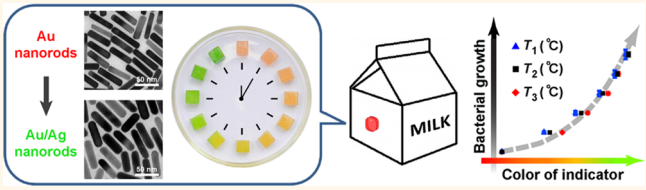


**KEYWORDS:** chronochromism · kinetic synchronicity · noble metal nanocrystals · perishables · localized surface plasmon resonance · time–temperature indicators

New opportunities in a number of technological realms have emerged with the rapid development of plasmonic nanocrystals.[1−7] Some original, unconventional examples among them are of particular significance and elegance, such as high-dimensional optical storage,[8,9] plasmonic nanotweezers,[10,11] and plasmonic collimators for lasers.[12] In these works, plasmonic Au and Ag nanostructures, profiting from their rich plasmonic modes, extraordinarily large absorption/scattering cross sections, and inherent chemical inertness, endow the constructed devices with unparalleled functionalities and excellent robustness. Here in this article, we demonstrate that plasmonic metal nanocrystals can be employed for another important niche application, namely, time–temperature indicator[13−15] for perishable products, where the properties of plasmonic nanocrystals are essential for its efficacy and performance.

Perishable products, such as foods, beverages, and pharmaceuticals, are easy to spoil over time owing to microbial growth and/or (bio)chemical degradation. Hence, their shelf lives (or expiration dates) are crucial information for customers. However, currently, the shelf lives labeled on many product packages are commonly estimated on the basis of several (over)simplified assumptions, one of them being that perishables are preserved at a presumed constant temperature, typically around 4 °C for foods. This is not always true in real situations since perishables during their custody chain (including storage, distribution, and consumption) would almost inevitably experience temperature variations, and temperature is a well-known critical factor that affects product quality. As a result, it is unsurprising to often find perishables already deteriorated even *within* their so-stated "shelf lives" if they are not properly handled and preserved. Therefore, the

* Address correspondence to sun@pku.edu.cn, jfwang@phy.cuhk.edu.hk, xingchen@pku.edu.cn, yan@pku.edu.cn.

Received for review March 12, 2013 and accepted April 29, 2013.

**Published online April 29, 2013**
10.1021/nn401266u

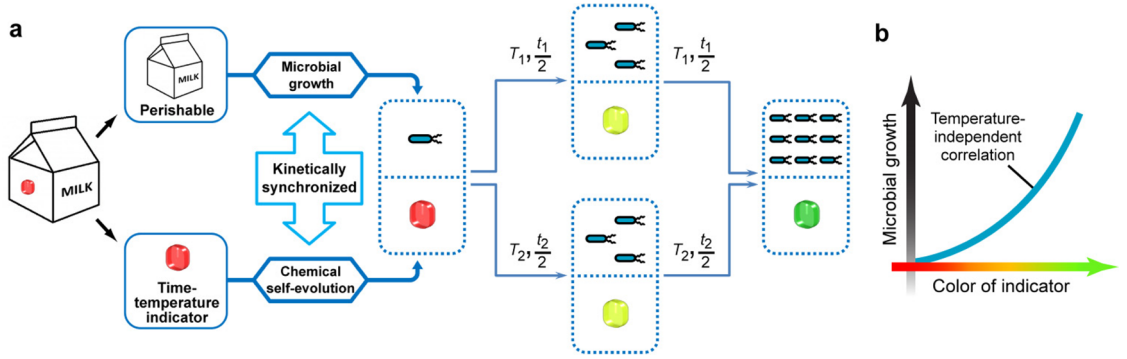


**Figure 1. Schematic illustrating the expected "bio−chemo" synchronicity. (a) Microbial growth in the perishable product and the chemical chronochromic self-evolution of the TTI are always kinetically synchronized, regardless of the temperature history. *T* and *t*, respectively, represent temperature and time duration. (b) Temperature-independent correlation between the magnitude of microbial growth and the color of TTI.**

credibility of current shelf life labels is questionable, which can be a major (sometimes even lethal) threat to public health.

To address this issue, the technique of TTI has been proposed[13] and is still under active development.[14,15] One major type of TTIs is electronics-based, represented by data loggers and radio frequency identification chips.[16] Deployed alongside products during transit, electronic TTIs can track and document the temperature history and translate it into the quality loss. However, these digital TTIs are generally expensive and therefore hardly applicable to each individual product item. A second type of TTIs resorts to physicochemical reactions, such as dye diffusion, enzymatic hydrolysis, and polymerization.[14,15] In addition, a TTI based on the plasmon shift of triangular Ag nanoplates caused by the spontaneous rounding of the sharp corners has also been reported.[17] By virtue of their relatively low cost, they can therefore be individually mounted on each product item and record the entire manufacturer-to-consumer custody chain. However, in general, the kinetic features (including both the kinetic rate and activation energy) of these chemical TTIs can hardly be widely tailored,[14,15,17] making them not as "programmable" as electronic ones. Hence, commonly, each type of chemical TTI can only cater specifically to a limited range of products. The limitations encountered with electronic and chemical TTIs make it very important to develop a general, unified, yet cost-effective technique that can track and archive the entire temperature history for each single product item and can simultaneously indicate the quality status in an easy-to-read manner. Notably, our TTI protocol, constructed based on the extremely sensitive dependence of the plasmon resonance on the shape and composition of bimetallic nanocrystals, has an unprecedentedly wide kinetic programmability, as well as minimal expense and low toxicity. Our proof-of-principle experiments show that this TTI can be generally utilized to *track* perishable products, to kinetically *mimic* deteriorative processes therein, and accordingly to *indicate* the product quality through a multicolor change.

## RESULTS AND DISCUSSION

**Underlying Principle.** The basic design principle is simple. As a typical class of perishables, dairy products spoil easily owing to bacterial growth, and the growth rate of bacteria is strongly dependent on temperature. For instance, *Escherichia coli* (*E. coli*) multiplies more rapidly at higher temperatures in the typical range of 0−37 °C. Likewise, many chemical reactions also speed up at elevated temperatures. The temperature dependencies of the kinetics for microbial growth and chemical reactions are quite similar (phenomenologically, at least). Therefore, ideally, if the kinetic rate (here in this context, "rate" is defined as the physical quantity that is the reciprocal of time needed for a certain dynamically evolving system to complete a predefined process at a constant temperature) of a certain chemical reaction is *constantly* (that is, at any given temperature) equal to that of *E. coli* growth, the processes of the chemical evolution and microbial growth are then mathematically equivalent and kinetically synchronized (Figure 1) and therefore can be easily correlated (see Part A in the Supporting Information for the detailed derivation). We therefore can envisage the design of a smart tracking tag based on the chemical reaction for dairy products. The tag is attached to the product package to ensure that it undergoes the same temperature history. The tag can then, in principle, serve as an indicator for the product quality because now the magnitude of microbial growth is *correlated to* and *indicated by* how much the chemical system has evolved. In addition, for the convenience of information readout, the chemical smart tag is preferred to exhibit color changes during evolution (that is, chronochromism[18]), so as to be readily discerned by naked eyes.

**Chronochromism during Ag Overgrowth on Au Nanorods and the Programmability of Its Kinetic Rate.** Considering the requirements above, we explored a number of chemical reactions and finally decided to employ the

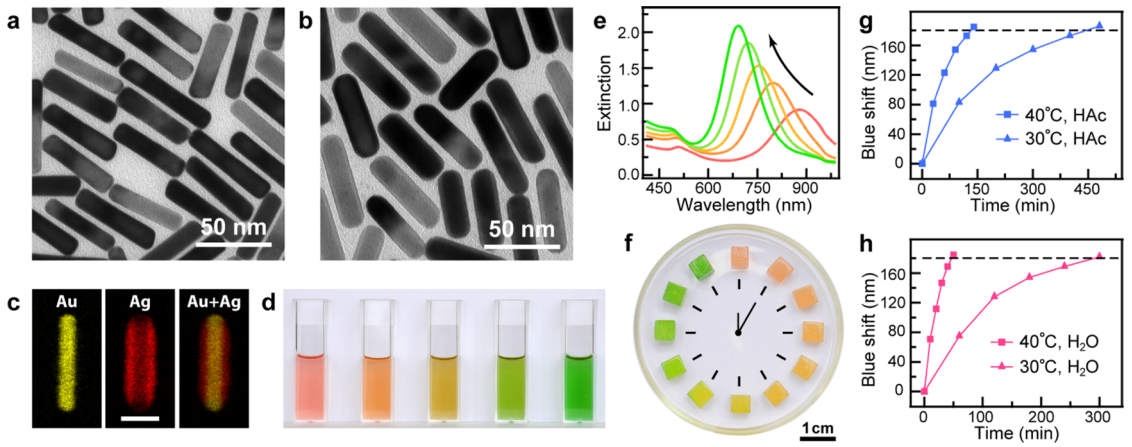


**Figure 2. Chronochromic evolution from Au nanorods to Au/Ag nanorods. (a,b) Transmission electron microscopy images of the Au and Au/Ag nanorods, respectively. (c) Energy-dispersive X-ray elemental mapping images for a typical Au/Ag nanorod. The scale bar represents 20 nm. (d) Photograph showing the color change of the self-evolving colloidal solution during the reaction process (from left to right). The temporal intervals between the neighboring samples are dependent on temperature and other parameters. (e) Extinction spectra of the samples in (d), showing a continuous blue shift of the longitudinal plasmon band from 880 to 690 nm. (f) Photograph of the hydrogel cubes (~5 × 5 × 3 mm$^3$) arranged in a manner resembling a clock in a Petri dish, illustrating the red-to-green chronochromic performance. (g,h) Plots of the blue shifts of the longitudinal plasmon band *versus* time for the acidified sample and the blank sample at 40 and 30 °C. The horizontal dashed line represents a blue shift of 180 nm.**

reaction of epitaxial overgrowth of Ag shell on Au nanorods,[19,20] by virtue of its sharp-contrast chronochromic behavior and readily adjustable kinetic features (see Methods and Part B in Supporting Information for the experimental details). The Au nanorods of 12 ± 1 nm diameter and 60 ± 5 nm length (Figure 2a and the leftmost in Figure 2d), dispersed in cetyltrimethylammonium chloride (CTAC) solution, give a red color. They exhibit two extinction bands around 510 and 880 nm (Figure 2e) arising from the transverse and longitudinal plasmon resonances, respectively. When the Ag precursor, $AgNO_3$, and the reducing agent, ascorbic acid (AA), are introduced, the yielded Ag atoms are epitaxially deposited on the Au nanorods, producing core/shell-structured Au/Ag nanorods (Figure 2b,c). As the Ag shell thickens, the extinction band of the longitudinal plasmon resonance gradually shifts to shorter wavelengths, and the colloidal solution changes its color from the initial red to orange, yellow, greenish-yellow, and further to green when the longitudinal plasmon peak shifts to ~690 nm. Our previous studies have shown that Ag atoms are preferentially deposited on the side surface than at the ends.[20] This preferential side deposition has been ascribed to the idea that the surface area increase for the side deposition is smaller than that for the end deposition.[21] The spectral change and therefore the color change have also been carefully analyzed in our previous work.[20] They are known to be contributed by both the aspect ratio and composition variations. The solution color can evolve further to blue and even violet with prolonged reaction time, but in this work, we chose green as the final-state color because (i) green is of sharp contrast (probably the sharpest) to the initial red color, and (ii) green is the color to which human eyes are most sensitive. Of particular note, the color change performance can be essentially retained when the colloidal solution is solidified as agar hydrogels (Figure 2f), thus conducive to practical applications. In addition, the temporal duration of this "red-to-green" chronochromism at room temperature can be widely tuned from minutes to months by simply adjusting the reaction parameters, such as the concentrations of the Au nanorods, CTAC, AA, and the pH value (see Part C in Supporting Information for detailed discussion). Therefore, under specified conditions (*i.e.*, temperature and the concentrations of the relevant chemicals), the solution color can give an intuitive indication of time passage. Furthermore, when the red-to-green chronochromic rate (denoted as $R'$ hereafter) of the TTI is adjusted to equal the growth rate (denoted as $R$ hereafter) of *E. coli* at a fixed temperature, different colors then correspond to different magnitudes of the bacterial growth.

**Programmability of the Apparent Activation Energy.** Although the chronochromic evolution process can be easily synchronized with the bacterial growth at a certain fixed temperature $T_1$ (that is, $R' = R$ at $T_1$), for practical uses, temperature variation over time needs to be taken into consideration. It is therefore crucial to ensure that when temperature changes to an arbitrary $T_2$, the two processes are still synchronized (that is, $R' = R$ at $T_2$). In this regard, it is imperative to find means for tailoring the temperature dependency of $R'$, that is, the apparent activation energy $E_a$ for this particular chemical reaction. We found that the introduction of acetic acid HAc (or other weak acids or bases, in principle) can effectively alter the $E_a$ value. As shown in Figure 2g, for the samples introduced with a

certain amount of HAc, it takes 131 min at 40 °C for the longitudinal plasmon peak to blue shift by 180 nm and 443 min at 30 °C. For the blank samples that were introduced with an equal volume of water (Figure 2h), it takes 47 and 291 min, respectively. Thus, for the blank samples, $R'_{40°C}/R'_{30°C} = 6.2$, with $E_a$ estimated to be 144 kJ·mol$^{-1}$, while for the acidified samples, $R'_{40°C}/R'_{30°C} = 3.4$, with $E_a$ estimated to be 96 kJ·mol$^{-1}$. These results confirm that the introduction of HAc is an effective way for tuning the $E_a$ value (see Part D in Supporting Information for the corresponding mechanism). Furthermore, by adjusting the HAc/AA ratio, the $E_a$ value can be continuously tuned within a certain range. We found that by introducing different amounts of HAc and AA, the $R'_{(T+10)°C}/R'_{T°C}$ ratio can vary roughly from 2 to 15, which, according to Arrhenius equation, corresponds to an $E_a$ value ranging from 50 to 190 kJ·mol$^{-1}$. Notably, this range covers the typical $E_a$ values for almost all ambient-temperature deteriorative processes in foods (see Part E in Supporting Information for the detailed explanation).[14,15,22]

With the tunability of both $R'$ and $E_a$ (in other words, the kinetic programming flexibility) for the TTI verified, we sought to synchronize the TTI evolution with the bacterial growth process at two *arbitrary* temperatures between 0 and 37 °C. In this section, we chose 30 and 20 °C for a proof-of-principle demonstration.

**Determination of the Rates of the Bacterial Growth.** The growth rates of *E. coli* at 30 and 20 °C were investigated. Lysogeny broth was employed as a mimic of milk. *E. coli* inoculated in the broth were cultured in an incubator and counted *via* turbidimetry. We found that the optical density at 420 nm ($OD_{420}$) below 1.0 exhibits a characteristic exponential growth over time at both temperatures, as shown representatively in Figure 3 (see Part F in Supporting Information for more data). The calculations based on the fitting results show that the population of *E. coli* doubles every 1.01 ± 0.04 h at 30 °C and every 5.88 ± 0.25 h at 20 °C, indicating that $R_{30°C}/R_{20°C} \approx 5.8$.

**Synchronizing the TTI Evolution with the Bacterial Growth at Two Arbitrary Temperatures.** Subsequently, we adjusted the kinetics of the chronochromic TTI by varying the concentrations of AA and HAc. By a trial-and-error approach, an optimized recipe ensuring that $R'_{30°C}/R'_{20°C} \approx 5.8$ was found (Part B5 in Supporting Information). Prepared according to this optimized recipe, the colloidal solution was then incubated at 30 °C for 5 h, and the corresponding extinction spectra were recorded every 1.0 h. The longitudinal plasmon peak shifted from the initial 880 to 703 nm, as summarized in Figure 4a. Likewise, the solutions were incubated at 20 °C for 5 × 5.8 = 29.0 h, with extinction spectra recorded every 5.8 h (Figure 4b). We then, according to the kinetic rates $R$ determined in Figure 3 (summarized in Part F in Supporting Information), calculated the magnitudes of the bacterial growth $\ln(N_t/N_0)$, where $N_0$ and $N_t$ represent the populations of *E. coli*, respectively, at time 0 and $t$, and plotted the obtained values *versus* the blue shifts of the longitudinal plasmon peak. As shown in Figure 4c, at 30 and 20 °C, the correlations between $\ln(N_t/N_0)$ and the blue shift are very similar, demonstrating that the chemical evolution and bacterial growth processes are practically synchronized at both temperatures. The dashed curve in Figure 4c can then be regarded as the standard curve for the "bio−chemo" correlation for 30 and 20 °C.

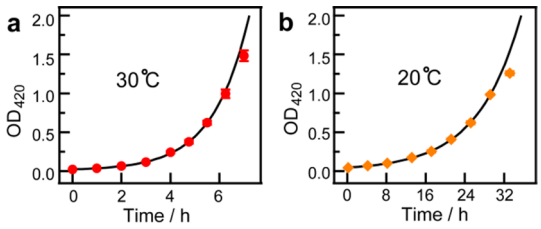


**Figure 3. E. coli growth. (a,b) Plots of $OD_{420}$ *versus* time at 30 and 20 °C, respectively.**

However, the results above do not necessarily guarantee the synchronicity at a third temperature $T_3$ because the $E_a$ value of a specific system may differ somewhat for different temperature ranges. Therefore, we chose 35 °C as a representative condition for further examination. The corresponding data are summarized in Figure 4d,e. The data obtained at 35 °C are seen to lie slightly above the standard curve, indicating that, at 35 °C, the TTI with the above recipe evolves slower than *E. coli* multiplies, which is also reflected by the colors of the TTI. As shown in Figure 4f, after incubation at 30 °C for 5.0 h, the TTI has already developed a greenish hue. Similar results are obtained for the condition of 20 °C for 29.0 h, confirming that the kinetic rate of the TTI approximately equals that of the bacterial growth ($R' \approx R$) at both 30 and 20 °C. However, after incubation at 35 °C for 2.60 h, the TTI has not turned green, indicating that $R' < R$ at 35 °C. Similarly, an asynchronicity of $R' > R$ is observed for 10 °C (Part G in Supporting Information).

**Achieving Synchronicity at Three or More Arbitrary Temperatures.** The issue of asynchronicity for $n$ ($n \geq 3$) temperatures can be resolved in two manners. First, we can resort to fabricating TTI arrays. By incorporating multiple TTIs (each with its own specific recipe) in an array, the indication accuracy can, in principle, be effectively improved. Second, we can further complicate the above recipe by introducing more proper weak acids (besides HAc) as coadjusting agents of the $E_a$ value. The validity of the latter was confirmed with the following experiments.

We further introduced a third weak acid, lactic acid (HLa), and managed to achieve the synchronicity at all three temperatures. Employing an optimized AA/HAc/HLa ratio (Part B6 in Supporting Information), we collected corresponding data at 30, 20, and

a

30°C for 5.0 h

| $t$ (h) | $\lambda$ (nm) | $\ln(N_t/N_0)$ |
|---|---|---|
| 0.0 | 880±1 | 0±0 |
| 1.0 | 800±2 | 0.685±0.027 |
| 2.0 | 757±1 | 1.370±0.054 |
| 3.0 | 738±1 | 2.055±0.081 |
| 4.0 | 720±2 | 2.740±0.109 |
| 5.0 | 703±1 | 3.425±0.136 |

b

20°C for 29.0 h

| $t$ (h) | $\lambda$ (nm) | $\ln(N_t/N_0)$ |
|---|---|---|
| 0.0 | 880±1 | 0±0 |
| 5.8 | 779±1 | 0.684±0.029 |
| 11.6 | 747±1 | 1.368±0.058 |
| 17.4 | 731±1 | 2.052±0.087 |
| 23.2 | 718±1 | 2.736±0.116 |
| 29.0 | 707±2 | 3.420±0.145 |

c

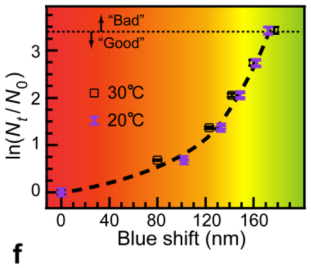


d

35°C for 2.60 h

| $t$ (h) | $\lambda$ (nm) | $\ln(N_t/N_0)$ |
|---|---|---|
| 0.00 | 880±1 | 0±0 |
| 0.52 | 818±2 | 0.683±0.066 |
| 1.04 | 778±1 | 1.366±0.131 |
| 1.56 | 751±1 | 2.050±0.197 |
| 2.08 | 733±1 | 2.733±0.263 |
| 2.60 | 717±1 | 3.416±0.328 |

e

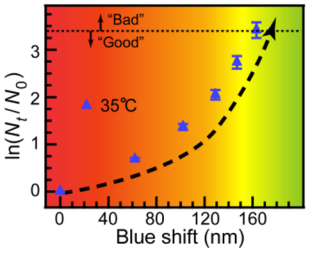


f

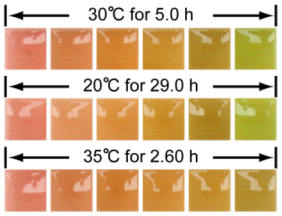


**Figure 4. Bio–chemo synchronicity. (a,b) Longitudinal plasmon peak wavelength ($\lambda$) and $\ln(N_t/N_0)$ varying over time at 30 and 20 °C, respectively. (c) Plot of $\ln(N_t/N_0)$ against the blue shift for both 30 and 20 °C. The horizontal dotted line indicates the quality differentiation between "Good" and "Bad", the position of which is (and can be, in principle) arbitrarily chosen. In addition, the error bars for the blue shifts are too small and thus omitted for clarity. (d) Longitudinal plasmon peak wavelength and $\ln(N_t/N_0)$ varying over time at 35 °C. (e) Plot of $\ln(N_t/N_0)$ against the blue shift for 35 °C. The dashed curve represents the data obtained at 30 and 20 °C in (c). (f) Photographs of the colloidal solutions in 10 × 10 mm$^2$ wells, each series from left to right corresponding to the times in (a,b,d), respectively. The bright parts in each photograph are due to the reflection from the concave surface of the colloidal solutions.**

a

30°C for 5.0 h

| $t$ (h) | $\lambda$ (nm) | $\ln(N_t/N_0)$ |
|---|---|---|
| 0.0 | 880±1 | 0±0 |
| 1.0 | 814±1 | 0.685±0.027 |
| 2.0 | 771±1 | 1.370±0.054 |
| 3.0 | 741±2 | 2.055±0.081 |
| 4.0 | 721±1 | 2.740±0.109 |
| 5.0 | 706±1 | 3.425±0.136 |

b

20°C for 29.0 h

| $t$ (h) | $\lambda$ (nm) | $\ln(N_t/N_0)$ |
|---|---|---|
| 0.0 | 880±1 | 0±0 |
| 5.8 | 797±1 | 0.684±0.029 |
| 11.6 | 762±1 | 1.368±0.058 |
| 17.4 | 734±1 | 2.052±0.087 |
| 23.2 | 720±2 | 2.736±0.116 |
| 29.0 | 707±1 | 3.420±0.145 |

c

35°C for 2.60 h

| $t$ (h) | $\lambda$ (nm) | $\ln(N_t/N_0)$ |
|---|---|---|
| 0.00 | 880±1 | 0±0 |
| 0.52 | 822±2 | 0.683±0.066 |
| 1.04 | 779±2 | 1.366±0.131 |
| 1.56 | 746±1 | 2.050±0.197 |
| 2.08 | 725±1 | 2.733±0.263 |
| 2.60 | 710±1 | 3.416±0.328 |

d

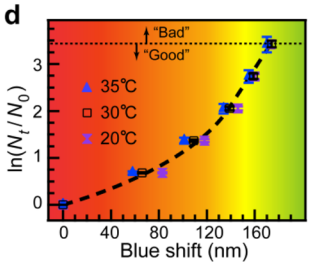


e

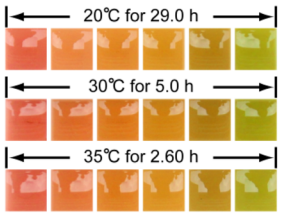


**Figure 5. Further improved bio–chemo synchronicity. (a–c) Longitudinal plasmon peak wavelength ($\lambda$) and $\ln(N_t/N_0)$ varying over time at 30, 20, and 35 °C, respectively. (d) Plot of $\ln(N_t/N_0)$ against the blue shift for 30, 20, and 35 °C. The horizontal dotted line indicates the quality differentiation between "Good" and "Bad", the position of which is (and can be, in principle) arbitrarily chosen. In addition, the error bars for the blue shifts are too small and thus omitted for clarity. (e) Photographs of the colloidal solutions in 10 × 10 mm$^2$ wells, each series from left to right corresponding to the times in (a–c), respectively. The bright parts in each photograph are due to the reflection from the concave surface of the colloidal solutions.**

35 °C (Figure 5a–c). As shown in Figure 5d, the bio–chemo correlations for these temperatures are basically superimposed, indicating that $R' \approx R$ at all three temperatures, which is also reflected by the colors of the TTI (Figure 5e). Therefore, by extrapolation, we can deduce that the bio–chemo synchronicity can be achieved simultaneously at $n$ temperatures by introducing $(n - 1)$ types of proper weak acids (for detailed explanation, please see Part H in Supporting Information).

**Cost, Safety, and Extendibility to Other Systems.** The TTIs presented here are also quite cost-efficient and eco-friendly. Although noble metals Au and Ag are used, their dosages are substantially low, around 10 $\mu g \cdot mL^{-1}$. The low dosages benefit from the extraordinarily large extinction coefficients of plasmonic metal nanocrystals,

which are typically $10^8$–$10^{10}$ $M^{-1}\cdot cm^{-1}$, 3–5 orders of magnitude higher than those of conventional dyes.[5–7,23] All of the other ingredients, including CTAC, AA, HAc, HLa, agar, and water, are inexpensive, and the fabrication procedures are in all-aqueous environment and basically under ambient conditions. When the TTI is solidified in agar hydrogel, the kinetics of the TTI in the solution and hydrogel phases are found to be nearly the same if the starting plasmon wavelengths are adjusted to be the same (Part I in Supporting Information). The same kinetics are ascribed to the highly porous nature of the hydrogel and that the rate-determining process in Ag overgrowth is the reduction of $Ag^+$ ions rather than the diffusion of the involved chemicals. For a single hydrogel cube shown in Figure 2f, which has a volume of ~70 $\mu$L, all of the chemicals involved therein are estimated to cost roughly US$0.002 (Part I in Supporting Information). As for safety concerns, CTAC, AA, HAc, HLa, and agar have already been extensively used in food, pharmaceutical, and cosmetic industries. The inert nature of gold also guarantees its nondeleteriousness. $AgNO_3$, though, can be corrosive (especially at high con centrations), yet in the presence of CTAC, $Ag^+$ cations will form insoluble and nonhazardous AgCl precipitate. In the recipe of the TTIs, an excessive amount of AA is introduced. It can protect the Ag shell against oxidation. For practical use, the TTIs need to be packaged and sealed. Therefore, external oxidants, such as atmospheric oxygen, are not expected to affect the performance of the TTIs. Therefore, by virtue of its minimal cost and low toxicity, this TTI hydrogel is disposable and can be readily implemented for real-world applications.

Also, the as-presented kinetically programmable TTI model can be extended to other aqueous Ag coating systems using the $Ag^+$/AA protocol, such as Au/Ag core/shell nanocubes[24–26] and Pd/Ag core/shell nanoplates.[27,28]

**Kinetics- *versus* Thermodynamics-Based Chemical Indicators.** Compared with conventional thermodynamics-based chemical indicators, such as pH paper, our chronochromic indicator is fundamentally different in that it is designed and executed on the basis of kinetics. The main differences between thermodynamics-based and kinetics-based indicators are summarized and discussed as follows: (i) While thermodynamics-based indicators see to analyte–substrate binding and equilibrium constants ($K_{eq}$), kinetics-based indicators see to kinetic rates ($R$) and activation energies ($E_a$) and hence are particularly suitable to those systems that are dynamic and evolving, rather than static and equilibrated. (ii) As a thermodynamic parameter, the equilibrium constant $K_{eq}$ for each specific reaction is generally dictated by the inherent nature of the involved chemicals, while the kinetic parameters ($R$ and $E_a$) for many reactions can be artificially and readily tailored. Therefore, the indication thresholds (or detection limits, in some cases) for kinetics-based indicators are quite flexible and adjustable. (iii) Thermodynamics-based indicators focus on the *individuality* of each particular analyte, which guarantees the selectivity of the indicators but at the same time also limits their applicability to different analytes. In contrast, kinetics-based indicators, as presented in our work, focus on the *commonality* in various systems (that is, the fact that for all perishables the deteriorative process generally accelerates at elevated temperatures). Combined with the kinetic programmability, our TTI model can be widely applied to indicate a myriad of dynamic processes. Moreover, the selectivity will not be essentially compromised because, for each specific target process, the recipe of the indicator can be specifically designed and formulated. (iv) Thermodynamics-based indicators normally require direct contact and sampling with the specimens of interest, and human operation is generally needed, while our chronochromic TTI is autonomous and self-evolving and can be left unattended. When deliberately designed and deployed, it can mimic the kinetic features of various target systems and hence indicate the product quality in an indirect and thus noncontact, nondestructive manner, which is of paramount importance where the intactness of product is emphasized.

## CONCLUSIONS

In summary, by exploiting the chronochromic behavior during the heteroepitaxy of Ag shell on Au nanorods, a plasmonic time–temperature indicator is designed and constructed, which gives a sharp-contrast red-to-green color change. The kinetic rate and apparent activation energy of this self-evolving system are widely tunable by simply varying the concentrations of the relevant reagents, guaranteeing a largely flexible programmability. This TTI can therefore be generally employed to track, mimic, and indicate the deterioration processes of numerous perishables. Proof-of-principle demonstrations prove that the self-evolution of the TTI and the growth process of *E. coli* can be well synchronized at three (or even more) arbitrary temperatures within the normal temperature window. If simply attached to product packages, the TTI can cover the entire manufacturer-to-consumer custody chain of each individual product item with little or even no human supervision and give a reliable indication of product quality and residual shelf lives regardless of the temperature history. Also, by virtue of the nature of the plasmonic noble metals Au and Ag, the TTIs are nontoxic, eco-friendly, and substantially low-cost. This new TTI model well meets the ASSURED (Affordable, Sensitive, Specific, User-friendly, Robust and rapid, Equipment-free, and Deliverable to end-users)[29] criteria proposed

by WHO. We believe that it holds the promise to be further developed into a unified and standardized protocol generally applicable to a vast number of perishable products and has great potential to revolutionize the current food/beverage/pharmaceutical/cosmetic industries.

## METHODS

**Materials.** Au nanorods were prepared following the well-established protocol of seed-mediated growth. *E. coli* (Trans1-Blue, Code #CD401, lot #G40330) was employed as the representative bacterium. Lysogeny broth was prepared according to the standard recipe. For more experimental details, please see Part B in Supporting Information.

**TTI Preparation.** For a typical preparation of the TTI in solutions, $AgNO_3$ solution (0.040 mL, 0.100 M) was added into CTAC solution (1.960 mL, 0.080 M), yielding a turbid suspension. To the suspension were sequentially added AA solution (1.000 mL, 1.136 M), Au nanorod solution (5.000 mL, extinction value = 3.00 at the longitudinal plasmon wavelength of 880 nm in a 1 cm cuvette), and water (8.000 mL). The mixed solution was incubated at various temperatures for different durations.

For a typical preparation of the TTI in hydrogel, to CTAC solution (1.960 mL, 0.080 M) was added agar powder (0.500 g). The suspension was stirred and heated over 80 °C until agar was fully dissolved. Under heating and vigorous stirring, to the solution were quickly added $AgNO_3$ solution (0.040 mL, 0.100 M), AA solution (1.500 mL, 1.136 M), Au nanorod solution (5.000 mL, the same concentration as above), and water (8.000 mL). The suspension was quickly transferred into a Petri dish and cooled at −10 °C in a refrigerator for 3 min, forming an opaque hydrogel plate. The plate was then sliced into small cubes and preserved under 35 °C for different durations.

**Characterizations.** The extinction spectra of the solution samples and the optical density values of Lysogeny broth were recorded on a UV-3100 spectrophotometer (Shimadzu). Transmission electron microscopy images were taken on an FEI TEM (Tecnai G2 Spirit Twin). Energy-dispersive X-ray elemental mapping images were taken on an FEI STEM/TEM (Tecnai G2 F20 S-Twin FA). The solutions and Lysogeny broth were incubated in a constant-temperature shaker (Shiping, China, SPH-200F).

*Conflict of Interest:* The authors declare no competing financial interest.

*Acknowledgment.* This work was supported by National Natural Science Foundation of China (Ref. Nos. 20931160429 and 21229101), Hong Kong Research Grants Council (GRF, Ref. No. CUHK403211, Project Code 2130277), and National Basic Research Program of China (Ref. No. 2009CB930303). C.Z. particularly thanks H.Y. Liu for helpful discussion and Q. Li and J.X. Wang for the help in recording the electron microscopy images and photographs.

*Supporting Information Available:* Detailed interpretation of the basic principles, methods, and materials, further discussion of the kinetic programmability, growth rates of *E. coli* at different temperatures, and assessment of material expense. This material is available free of charge *via* the Internet at http://pubs.acs.org.

## REFERENCES AND NOTES

1. Giannini, V.; Fernández-Domínguez, A. I.; Heck, S. C.; Maier, S. A. Plasmonic Nnaoantennas: Fundamentals and Their Use in Controlling the Radiative Properties of Nanoemitters. *Chem. Rev.* **2011**, *111*, 3888–3912.
2. Morton, S. M.; Silverstein, D. W.; Jensen, L. Theoretical Studies of Plasmonics Using Electronic Structure Methods. *Chem. Rev.* **2011**, *111*, 3962–3994.
3. Chen, H. J.; Shao, L.; Li, Q.; Wang, J. F. Gold Nanorods and Their Plasmonic Properties. *Chem. Soc. Rev.* **2013**, *42*, 2679–2724.
4. Daniel, M.-C.; Astruc, D. Gold Nanoparticles: Assembly, Supramolecular Chemistry, Quantum-Size-Related Properties, and Applications toward Biology, Catalysis and Nanotechnology. *Chem. Rev.* **2004**, *104*, 293–346.
5. Ghosh, S. K.; Pal, T. Interparticle Coupling Effect on the Surface Plasmon Resonance of Gold Nanoparticles: From Theory to Applications. *Chem. Rev.* **2007**, *107*, 4797–4862.
6. Hu, M.; Chen, J.; Li, Z.-Y.; Au, L.; Hartland, G. V.; Li, X.; Marquez, M.; Xia, Y. N. Gold Nanostructures: Engineering Their Plasmonic Properties for Biomedical Applications. *Chem. Soc. Rev.* **2006**, *35*, 1084–1094.
7. Wiley, B.; Sun, Y. G.; Xia, Y. N. Synthesis of Silver Nanostructures with Controlled Shapes and Properties. *Acc. Chem. Res.* **2007**, *40*, 1067–1076.
8. Zijlstra, P.; Chon, J. W. M.; Gu, M. Five-Dimensional Optical Recording Mediated by Surface Plasmons in Gold Nanorods. *Nature* **2009**, *459*, 410–413.
9. Chon, J. W. M.; Bullen, C.; Zijlstra, P.; Gu, M. Spectral Encoding on Gold Nanorods Doped in a Silica Sol−Gel Matrix and Its Application to High-Density Optical Data Storage. *Adv. Funct. Mater.* **2007**, *17*, 875–880.
10. Wang, K.; Schonbrun, E.; Steinvurzel, P.; Crozier, K. B. Trapping and Rotating Nanoparticles Using a Plasmonic Nano-Tweezer with an Integrated Heat Sink. *Nat. Commun.* **2011**, *2*, 249.
11. Juan, M. L.; Righini, M.; Quidant, R. Plasmon Nano-optical Tweezers. *Nat. Photonics* **2011**, *5*, 349–356.
12. Yu, N.; Fan, J.; Wang, Q. J.; Pflügl, C.; Diehl, L.; Edamura, T.; Yamanishi, M.; Kan, H.; Capasso, F. Small-Divergence Semiconductor Lasers by Plasmonic Collimation. *Nat. Photonics* **2008**, *2*, 564–570.
13. Byrne, C. H. Time Temperature Indicators—State of the Art. *Food Technol.* **1976**, *30*, 66–68.
14. Robertson, G. L. *Food Packaging: Principles and Practice*, 3rd ed.; CRC Press, Taylor & Francis Group: Boca Raton, FL, 2013; pp 415−418.
15. Tijskens, L. M. M.; Hertog, M. L. A. T. M.; Nicolaï, B. M. *Food Process Modelling*; CRC Press-Woodhead Publishing: Cambridge, 2001; pp 402−431.
16. Tao, H.; Brenckle, M. A.; Yang, M.; Zhang, J.; Liu, M.; Siebert, S. M.; Averitt, R. D.; Mannoor, M. S.; McAlpine, M. C.; Rogers, J. A.; *et al.* Silk-Based Conformal, Adhesive, Edible Food Sensors. *Adv. Mater.* **2012**, *24*, 1067–1072.
17. Zeng, J.; Robers, S.; Xia, Y. N. Nanocrystal-Based Time−Temperature Indicators. *Chem.—Eur. J.* **2010**, *16*, 12559–12563.
18. Bamfield, P.; Hutchings, M. G. *Chromic Phenomena: Technological Applications of Colour Chemistry*, 2nd ed.; RSC Publishing: Cambridge, 2010; pp 114−116.
19. Okuno, Y.; Nishioka, K.; Kiya, A.; Nakashima, N.; Ishibashi, A.; Niidome, Y. Uniform and Controllable Preparation of Au−Ag Core−Shell Nanorods Using Anisotropic Silver Shell Formation on Gold Nanorods. *Nanoscale* **2010**, *2*, 1489–1493.
20. Jiang, R. B.; Chen, H. J.; Shao, L.; Li, Q.; Wang, J. F. Unraveling the Evolution and Nature of the Plasmons in (Au Core)−(Ag Shell) Nanorods. *Adv. Mater.* **2012**, *24*, OP200–OP207.
21. Li, Q.; Jiang, R. B.; Ming, T.; Fang, C. H.; Wang, J. F. Crystalline Structure-Dependent Growth of Bimetallic Nanostructures. *Nanoscale* **2012**, *4*, 7070–7077.
22. Taoukis, P. S.; Koutsoumanis, K.; Nychas, G. J. E. Use of Time−Temperature Integrators and Predictive Modelling for Shelf Life Control of Chilled Fish under Dynamic Storage Conditions. *J. Food Microbiol.* **1999**, *53*, 21–31.
23. Ming, T.; Chen, H. J.; Jiang, R. B.; Li, Q.; Wang, J. F. Plasmon-Controlled Fluorescence: Beyond the Intensity Enhancement. *J. Phys. Chem. Lett.* **2012**, *3*, 191–202.
24. Ma, Y. Y.; Li, W. Y.; Cho, E. C.; Li, Z. Y.; Yu, T.; Zeng, J.; Xie, Z. X.; Xia, Y. N. Au@Ag Core−Shell Nanocubes with Finely Tuned

and Well-Controlled Sizes, Shell Thicknesses, and Optical Properties. *ACS Nano* **2010**, *4*, 6725–6734.
25. Cho, E. C.; Camargo, P. H. C.; Xia, Y. N. Synthesis and Characterization of Noble-Metal Nanostructures Containing Gold Nanorods in the Center. *Adv. Mater.* **2010**, *22*, 744–748.
26. Gandra, N.; Portz, C.; Singamaneni, S. Bimetallic Janus Nanostructures *via* Programmed Shell Growth. *Nanoscale* **2013**, *5*, 1806–1809.
27. Huang, X. Q.; Tang, S. H.; Mu, X. L.; Dai, Y.; Chen, G. X.; Zhou, Z. Y.; Ruan, F. X.; Yang, Z. L.; Zheng, N. F. Freestanding Palladium Nanosheets with Plasmonic and Catalytic Properties. *Nat. Nanotechnol.* **2011**, *6*, 28–32.
28. Huang, X. Q.; Tang, S. H.; Liu, B. J.; Ren, B.; Zheng, N. F. Enhancing the Photothermal Stability of Plasmonic Metal Nanoplates by a Core−Shell Architecture. *Adv. Mater.* **2011**, *23*, 3420–3425.
29. Peeling, P. W.; Holmes, K. K.; Mabey, D.; Ronold, A. Rapid Tests for Sexually Transmitted Infections (STIs): The Way Forward. *Sex. Transm. Infect.* **2006**, *82*, v1–v6.